8th International Conference on Power Electronics - ECCE Asia
May 30-June 3, 2011, The Shilla Jeju, Korea

# A Novel Method to Compensate Non-Linearity of Inverter in Sensorless Operation of PMSM

Yongsoon Park and Seung-Ki Sul

School of Electrical Engineering & Computer Science, Seoul National University, Seoul, Korea

yongsoon@eepel.snu.ac.kr

***Abstract*—The non-linearity of an inverter can be modeled as the distorted voltages. A novel method utilizing the trapezoidal voltages is proposed to cancel out the distorted voltages by the non-linearity. By modulating the shape of the trapezoid, the harmonic distortions in the output currents and the voltage references can be reduced. An integral controller is employed to modulate the trapezoid with simple signal processing. To evaluate the effectiveness of the propose method, the conventional methods are compared through the experimental results.**

***Index Terms*—non-linearity of inverter, permanent magnet synchronous motor, sensorless control**

## I. INTRODUCTION

The non-linearity of an inverter can be regard as the voltage differences between voltage references and actual outputs in Voltage Source Inverter (VSI). However, in a sensorless control system of Permanent Magnet Synchronous Motor (PMSM), the voltage references are utilized to estimate the angular position of rotor-flux instead of the actual voltages [1, 2]. Hence the non-linearity of the inverter, that means the voltage differences, can affect the performance of the sensorless control system.

Furthermore, the harmonic distortions in output currents arise from the non-linearity of the inverter. Those distortions not only result in more ohmic losses, but also cause torque ripples and speed fluctuation. Because the distortions are mainly low order harmonics, the problem can be worsened in the sensorless control system. Namely, the harmonics, which are reflected on the estimated angle and speed of the sensorless control, deteriorate the efficiency and stability of the system.

The non-linearity of the inverter is originated from some practical characteristics; preset dead-time, switching delays, parasitic capacitances and on-state voltages. A lot of researches have been executed, which focus on how to compensate those factors [3-9]. However, because these compensations are based on limited data for certain operating conditions, it is difficult to guarantee their effectiveness for overall operating conditions.

Meanwhile, the other attempts have been carried out using the disturbance observer [10-12]. The non-linearity of the inverter has been considered as the disturbance voltages to be mitigated, and the disturbance observer has been used to estimate the disturbance voltages. These methods are expected to be effective to mitigate the disturbances in the wide range of operating condition regardless of their physical reasons. However, the electrical parameters, which are required to compose the observer, also vary according to the operating conditions. Therefore, the methods based on the observer are not totally independent with the operating conditions. Moreover, the accuracy of the rotor angle, which is crucial information to the observer, is not definite in the sensorless control system.

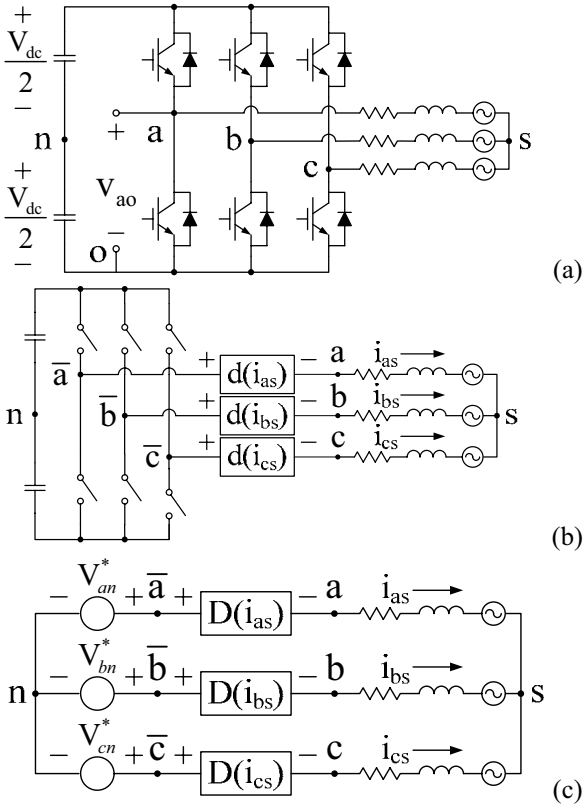


Fig. 1 Modeling of inverter circuit for a sampling period

A novel method to compensate the non-linearity of the inverter is proposed in this paper. The proposed method is analogous with the method of the disturbance observer in the point that the non-linearity is considered as the distorted voltage. However, the compensating voltage can be adaptively modulated under different load conditions without the aid of any observers. The effectiveness of the proposed method is evaluated by a series of experiments.

## II. COMPENSATING VOLTAGES

To explain the principle of the compensation, the inverter circuit for a sampling period is modeled at first. Fig. 1-a shows the typical circuit of three-phase inverter. Some practical properties, on-state voltages and parasitic capacitances, can be isolated as shown in Fig. 1-b. Then,



978-1-61284-957-7/11/$26.00 ©2011 IEEE

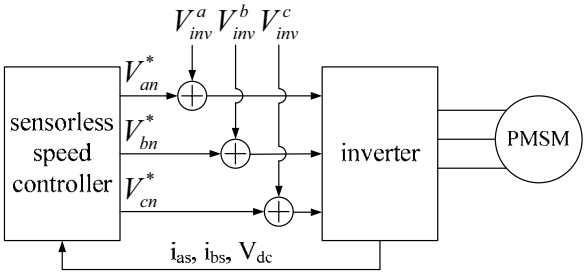


Fig. 2 Feed-forward voltages for compensation

the inverter itself consists of ideal switches with the non-linear loads.

In the space vector PWM (SVPWM) [14], one sampling period can be the minimum unit to synthesize the voltage output according to its reference. The circuit in Fig. 1-b for a sampling period can be translated into Fig. 1-c, where the effects of the dead-time and switching delays are also included.

The mechanism of the compensation is clarified in Fig. 1-c combined with Fig. 2. If the compensating voltage, $V^a_{inv}$ in Fig. 2, eliminates the effect of the non-linear voltage, $D(i_{as})$ in Fig 1-c, the reference pole voltage, $V^*_{an}$ in Fig. 1-c, is equal to the actual pole voltage, $V_{an}$ in Fig. 1-c. This means that the non-linearity of the inverter is cancelled out. Therefore, it is crucial how to obtain those feed-forward voltages accurately.

### *A. Sign Definition of Distorted Voltage by Inverter*

In general, the dead-time is employed to prevent the arm-short for the switching of the active switches in an arm of the inverter. It is shown in Fig. 3 how the dead-time for a switching period is implemented and affects the terminal voltages together with the parasitic capacitances parallel to the switches. The terminal voltage, $v_{ao}$, is also defined in Fig. 1-a. In Fig. 3, $T_d$ is the dead-time, and $T^*_a$ is the reference interval calculated from the reference voltage.

Depending on the sign of the output current, $i_{as}$, the volt-second distortion by the dead-time, designated as 'Y' in Fig. 3, can be loss or gain when the actual interval, $T_a$, is compared with the reference interval [6, 7]. If this volt-second is averaged for a switching period, the distortion by the dead-time can be expressed as follows.

$$\begin{cases} V_{ao} = V^*_{ao} - V_d, & i_{as} > 0 \\ V_{ao} = V^*_{ao} + V_d, & i_{as} < 0 \end{cases} \rightarrow \begin{cases} V^*_{ao} = V_{ao} + V_d, & i_{as} > 0 \\ V^*_{ao} = V_{ao} - V_d, & i_{as} < 0 \end{cases} \quad (1)$$

, where $V_d$ is the voltage distortion by the dead-time.

The distortion by the dead-time can be considered as the passive load to the voltage reference in (1). In addition, the switching device has conductive resistance and initial voltage drop at the starting of the current-conduction, which can be called as the voltage drop of the switch at conducting. Hence, the total sign of the distorted voltage by the dead-time and the on-state voltages can be defined as shown in Fig. 1-c in addition to (2).

$$\begin{cases} D(i_{as}) > 0, & if \quad i_{as} > 0 \\ D(i_{as}) < 0, & if \quad i_{as} < 0 \end{cases} \quad (2)$$

In Fig. 3, the effects of the parasitic capacitances can also be explained [8, 9]. Those effects are revealed in the regions indicated by 'Z'. If the parasitic capacitances are small enough to be ignored, the switching state of one leg during 'Z' is almost directly commutated from 'state1' to 'state2'. However, otherwise, another stage, 'state3', influences the voltage output when the output current is close to zero, so that the solid boundary of 'Z' approaches to the dashed boundary of 'Z'. Because the averaged volt-second of this phenomenon has opposite sign to that of the dead-time, the net effect of them is almost vanished in

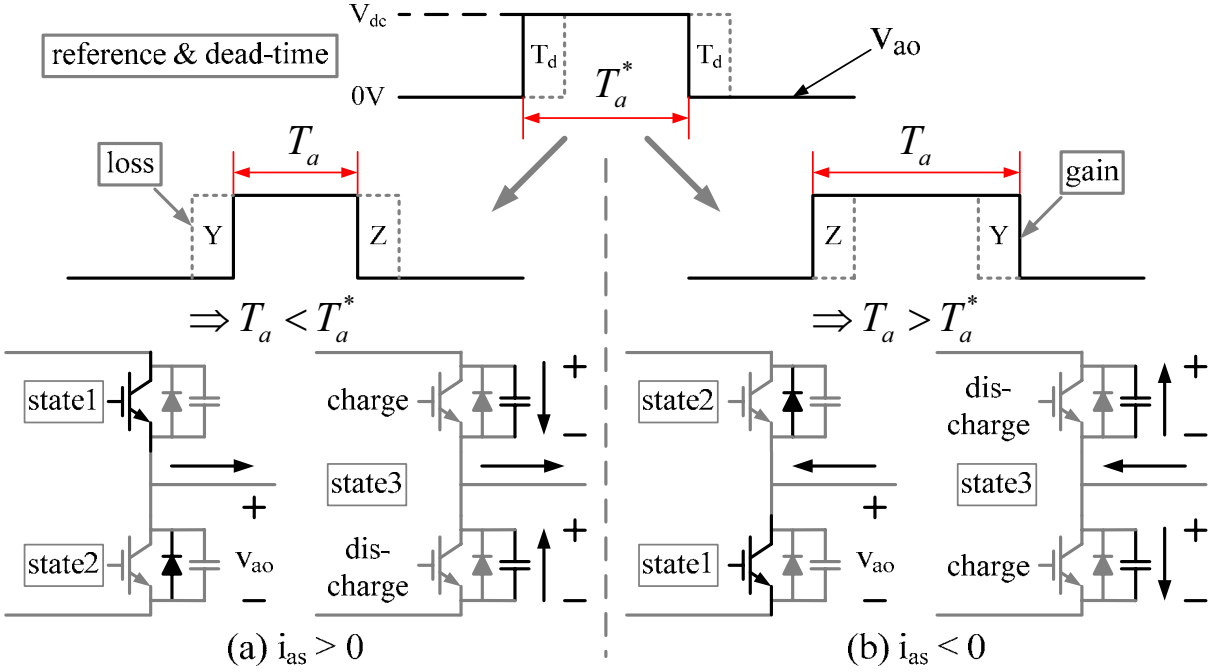


Fig. 3 Effects of dead-time and parasitic capacitances

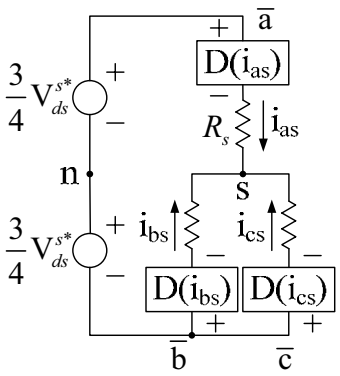


Fig. 4 Inverter circuit at stationary condition

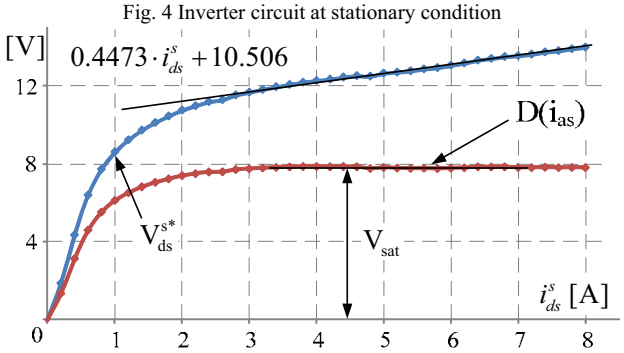


Fig. 5 Distorted voltage at stationary condition

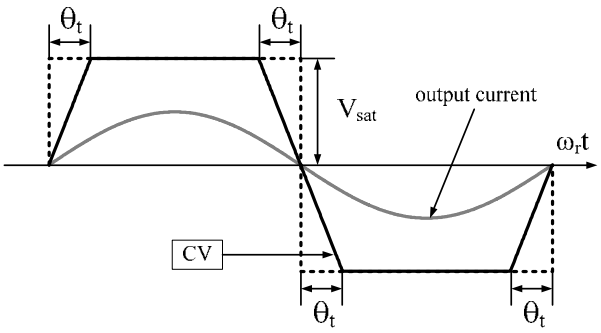


Fig. 6 Modulation of compensating voltage

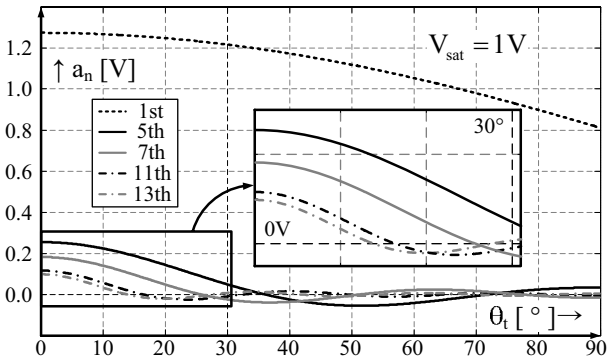


Fig. 7 Fourier coefficients of trapezoidal voltage according to angle

the case that the output current is almost zero. However, the effects of capacitances are maximally limited to the 'Z' region. Thus, though the amount of the distorted voltage may be different, (2) is still held even if the parasitic capacitances are considered.

### B. Distorted Voltage at Stationary Condition

The distorted voltage by the non-linearity of the inverter can be measured at standstill based on the circuit in Fig. 1-c. At stationary condition of PMSM, Fig. 1-c is simplified into Fig. 4 with SVPWM when the d-axis current in the stationary reference frame is regulated as a non-zero value. From Fig. 4, the distorted voltage can be calculated by Kirchoff's voltage law as follows.

$$D(i_{as}) = \frac{3}{4} \cdot (V_{ds}^{s*} - R_s \cdot i_{ds}^{s}) \tag{3}$$

$$\left|D(i_{as})\right| = \left|D(i_{bs})\right| = \left|D(i_{cs})\right| = const. \tag{4}$$

, where $V_{ds}^{s*}$ and $i_{ds}^{s}$ are the d-axis voltage reference and current in the stationary reference frame, respectively. And (3) is derived under the assumption of (4), that is, the magnitude of the distorted voltage is the same at any phase.

In Fig. 5, the experimental results are shown, where the voltage references are captured according to the current. Because the effect of the parasitic capacitances is dominant near zero-current, the equivalent resistance of the inverter, which is the slope of the voltage-reference curve according to the current in Fig. 5, should be computed at sufficiently large current region. Then, employing that resistance, the distorted voltages are calculated by (3) as shown in Fig. 5.

### C. Shape of Compensating Voltage (CV)

The distorted voltages measured in Fig. 5 have been exploited to compensate the non-linearity of the inverter. One method has used only the saturated voltage [3], $V_{sat}$ in Fig. 5. And the other employs the look-up table [4], storing the whole data up to the saturation in Fig. 5.

In this paper, the trapezoidal voltage, CV in Fig. 6, is proposed to cancel out the non-linearity of the inverter. This voltage is in phase with the output current. If the trapezoidal angle, $\theta_t$ in Fig. 6, is zero, the proposed method is equivalent to the method only using the saturated voltage. Furthermore, this trapezoid also can be the approximation to the compensating voltage of the method employing the look-up table. The evident difference is that the trapezoidal angle is changed depending on the operating conditions in this proposed method.

The meaning of the trapezoidal angle is obvious in Fig. 7, which shows the coefficients of the Fourier series for the trapezoid when the saturation voltage is 1V. Up to 30 degrees, the fundamental component only decreases by 4.5% while the other harmonics, $5^{th}$, $7^{th}$, $11^{th}$, and $13^{th}$, are changed drastically. Then, the modification of the trapezoidal angle, up to 30 degrees, indicates the magnitudes of the low order harmonics can be modulated. If this modulation is appropriate, the harmonic distortions of the output currents and the voltage references can be reduced effectively, regardless of their physical origins.

### D. Modulation of Compensating Voltage

There are two reasons to find the phase of the output current. One is to synchronize the compensating voltage with the output current, and the other is to observe the harmonic distortions of the output current. This phase information can be obtained employing the Phase Locked

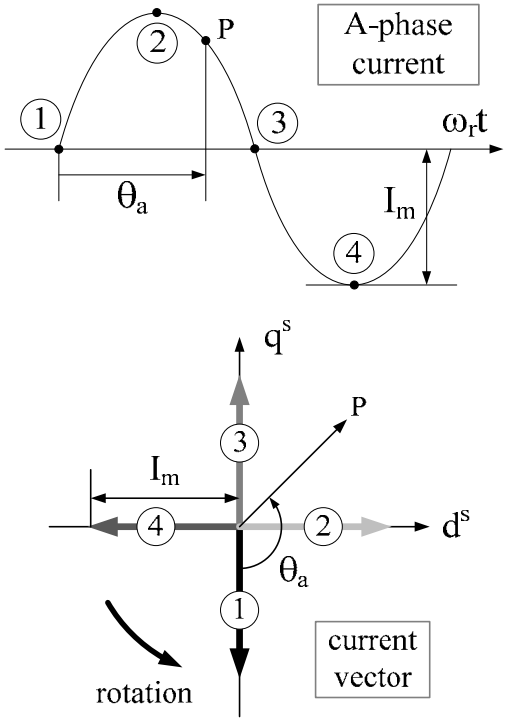


(a)

(b)

Fig. 8 A-phase current and current vector

Loop (PLL) [13].

To deal with the phase, an orientation point must be defined at first. It is defined as the zero-crossing of the A-phase current with the positive slope, the point ① in Fig. 8-a. Because the three-phase current can be depicted as a rotating vector in the stationary reference frame, the angle corresponding to the orientation point can be determined spatially. If the A-phase current is given in Fig. 8-a, the corresponding current vectors are depicted as shown in Fig. 8-b. Then, the angle is defined as $\theta_a$ in Fig. 8.

Then, the d- and q- axis currents in the frame, synchronized with the A-phase, are obtained from the three-phase current as follows.

$$\begin{bmatrix} i_{ds}^a \\ i_{qs}^a \end{bmatrix} = \frac{2}{3} \cdot \begin{bmatrix} \sin\theta_a & \sin\theta_{a1} & \sin\theta_{a2} \\ \cos\theta_a & \cos\theta_{a1} & \cos\theta_{a2} \end{bmatrix} \begin{bmatrix} i_{as} \\ i_{bs} \\ i_{cs} \end{bmatrix} \quad (5)$$

$$\theta_{a1} = \theta_a - \frac{2\pi}{3}, \theta_{a2} = \theta_a + \frac{2\pi}{3} \quad (6)$$

The q-axis current in the synchronous frame is important, where the low order harmonics can be seen without dc value. For instance, let's assume the 5th order harmonics are given in (7). By (5) and (6), the q-axis current in the synchronous frame can be deduced as (8).

$$i_{as5} = I_5 \sin 5\theta_a,\ i_{bs5} = I_5 \sin 5\theta_{a1},\ i_{cs5} = I_5 \sin 5\theta_{a2} \quad (7)$$

$$i_{qs5}^a = I_5 \cdot \sin 6\theta_a \quad (8)$$

The current-magnitude of (7) is the same with that of (8), while the harmonic order is changed from 5 to 6 in (8). The similar result is obtained in the case of the 7th order harmonics. Then, the harmonic distortions, 5th and 7th, in the output currents are expressed in the q-axis of the synchronous frame as (9).

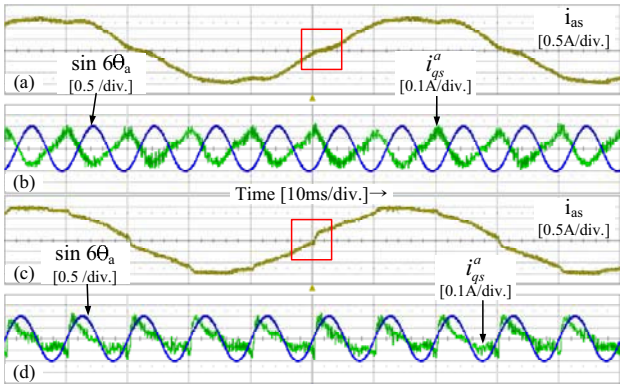


Fig. 9 Harmonic currents depending on compensations, 500r/min, no load: (a), (b) – larger trapezoidal angle → less-compensation, (c), (d) – smaller trapezoidal angle → over-compensation

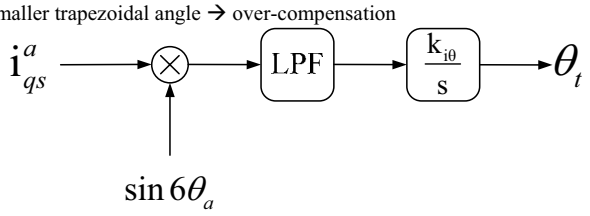


Fig. 10 Controller for trapezoidal angle

$$i_{qsh}^a = (I_5 + I_7) \cdot \sin 6\theta_a \quad (9)$$

, where $I_k$ is the magnitude of $k^{th}$ order harmonic.

It is important to detect the polarity of the current harmonic, because the polarity can be the criterion of the modulation for the trapezoidal angle in Fig. 6. For the detection of the polarity, the additional signal processing should be done as (10), where LPF means Low Pass Filtering of the signal.

$$LPF[\, i_{qs}^a \cdot \sin 6\theta_a \,] \approx \frac{I_5 + I_7}{2} \quad (10)$$

According to the polarity of (10), the trapezoidal angle can be modulated. In Fig. 9-a, the A-phase current is clamped every zero-crossing. Then, the harmonics of the q-axis current in the synchronous frame is out of phase with $\sin 6\theta_a$, which means the polarity of (10) is negative. This is the case that the trapezoidal angle is too large, which means less-compensation.

On the other hand, the A-phase current is abruptly changed every zero-crossing in Fig. 9-b, and the harmonics of the q-axis current in the synchronous frame is in phase with $\sin 6\theta_a$. This is the case that the trapezoidal angle is too small, which means over-compensation. In this case, the polarity of (10) is positive.

Based on the above observation, the controller to modulate the trapezoidal angle can be designed as shown in Fig. 10. The upper limit for the angle is select as about 30 degrees, because the negative correlation between the trapezoidal angle and the magnitudes of the harmonics doesn't persist over 30 degrees as shown in Fig. 7.

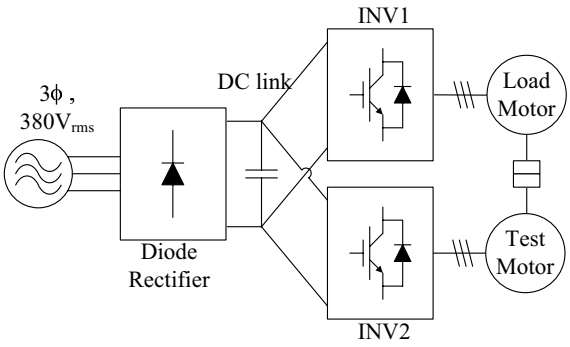

Fig. 11 Conceptual circuit of experimental set-up

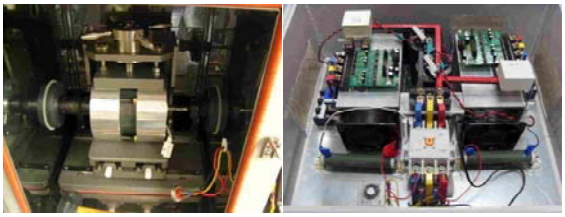
Fig. 12 Test motor and inverter

## III. EXPERIMENTS

### A. Experimental set-up

The experimental hardware can be explained with the conceptual circuit diagram as shown in Fig. 11. Two motors are coupled with each other mechanically, and both inverters share the dc-link, comes from a 3ϕ-380V$_{rms}$ voltage-source via a diode rectifier. The 75A-1200V IGBT modules are used as the switches of the inverters.

The motor under the test in Fig. 11 is a 6.8kW Interior Permanent Magnet Synchronous Motor (IPMSM). And the load motor is a 13kW Surface Mounted Permanent Magnet Synchronous Motor (SMPMSM). The test motor is controlled with the sensorless control method in [1], and a resolver is only employed to control the load motor.

To generate switching signals, the DSP board based on TMS320VC33 is used. And all control algorithms are implemented digitally with the DSP board. The periods of sampling and switching are respectively selected as 100μs and 200μs, that means 5kHz switching and double-sampling in a switching period. And the preset dead-time is 3μs.

### B. Target of experimental comparisons

The peak magnitude of the trapezoid is determined from the distorted voltage at stationary condition. The data previously shown in Fig. 5 are obtained from the inverter used in the experimental set-up. Then, the saturated level, which is the peak magnitude of the trapezoid, is computed as 7.88V for the given inverter.

Two other methods [3, 4], aforementioned in the section II-C, are considered as the comparison groups, because these methods are based on the same distorted voltage with the proposed method. For convenience, the method in [3], utilizes the saturated voltage only as the magnitude of the sign function of the output current, is designated as 'square method'. And the method in [4], employs the look-up table to determine the compensating voltage, is designated as 'table method'.

Both the output currents and the voltage references are compared in each case. Because the output torque is mainly generated by the fundamental output currents, more harmonics in the currents are regarded as additional losses and torque ripples at that operating condition.

As mentioned before, the purpose of the compensation is to remove the difference between the voltage references and the actual output of the inverter. With a balanced motor-load, balanced voltage references are to be observed if the non-linearity of the inverter is perfectly compensated. Then, the distortions in the voltage references also may be used as the criterion to evaluate the effectiveness of each method.

Furthermore, if the low order harmonics are included in the voltage references, the same harmonics may appear in the estimated- angle and speed. Because of the attempt to reduce the error between a speed reference and the estimated speed, the distortions at those harmonic frequencies in the current can be increased. This may worsen the stability of the sensorless control system.

### C. Experimental results

The correlation between the proposed method and conventional methods is well displayed in Fig. 13. With 4N·m load at 500r/min, the d-axis current in the rotor reference frame, $i^r_{ds}$, is regulated as zero. Unlike the d- and q- axis currents in the stationary reference frame, $i^s_{ds}$ and $i^s_{qs}$, the harmonic distortions are evident in the d-axis current of the rotor reference frame in Fig. 13.

Compared with the case of no compensation, the harmonic distortions are obviously mitigated after the proposed method is applied as shown in Fig. 13-d. Although the compensating voltage by the table method in Fig. 13-c also resembles the trapezoid, the result is totally different with Fig. 13-d. The data stored in the table are effective only in the certain operating conditions. The unsuitable influence of the trapezoidal angle is confirmed indirectly in Fig. 13-c.

However, the square method also exhibits excellent performance as shown in Fig. 13-b. This is because the trapezoidal angle of the proposed method converges to zero when the slope of the current near the zero-crossing is large enough. The physical meaning of this is that the effect of the parasitic capacitances almost disappears if the magnitude or frequency of the output current is sufficiently large. Therefore, the proposed method is analogous with the square method under the conditions, where the parasitic capacitances are negligible.

To demonstrate the distinct differences between the square method and the proposed method, the motor under the test is driven at 150r/min with no load in Fig. 14. This is the case that both the magnitude and frequency of the output current are small. Because of the dominant influence by the parasitic capacitances, the square method is not effective any more as shown in Fig. 14-b. Rather, the harmonic distortions are increased even compared with the case of no compensation.

Contrary to the other methods, the propose method still sustains its effectiveness as shown in Fig. 14-d. Because of

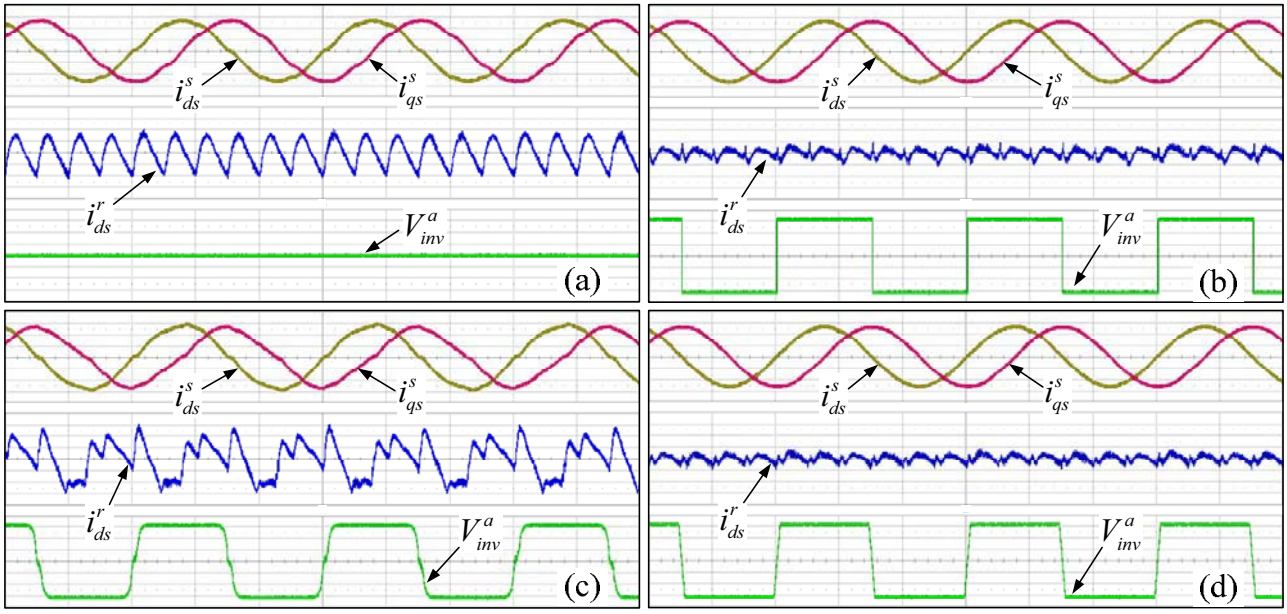


Fig. 13 Output currents and compensating voltages, 500r/min, 4N·m load:
(a) no compensation, (b) square method, (c) table method, (d) proposed method
$i_{ds}^s, i_{qs}^s$ [3A/div. , center: 0A] , $i_{ds}^r$ [0.25A/div. , center: 0A] , $V_{inv}^a$ [2.5V/div. , center: 0V], Time [20ms/div.]

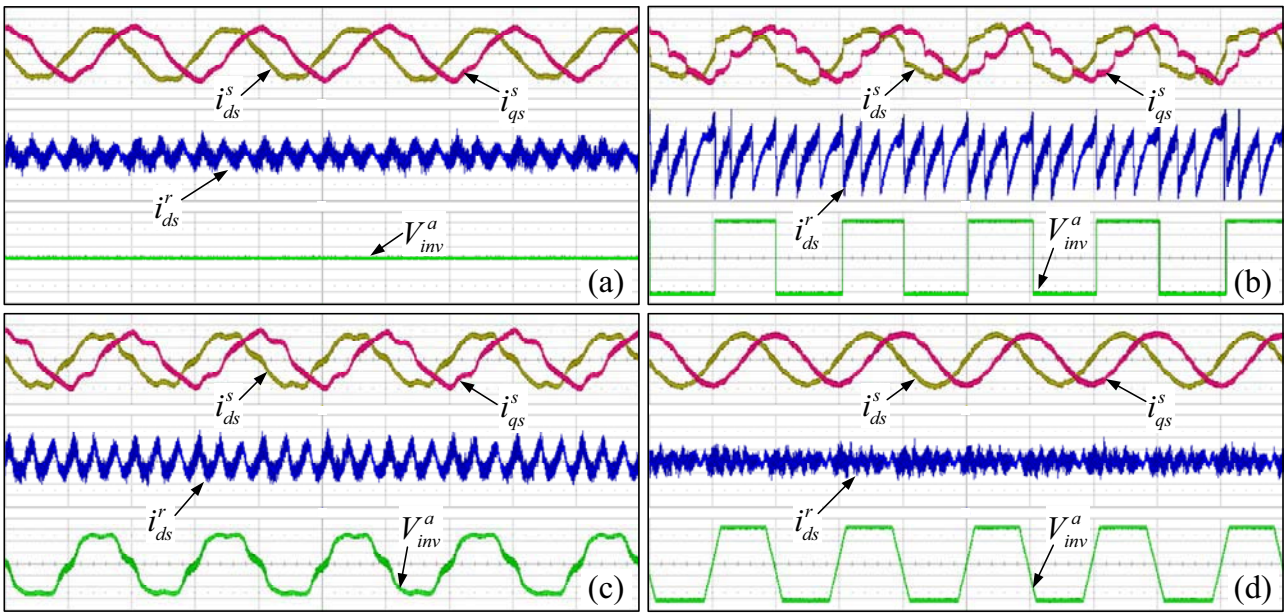


Fig. 14 Output currents and compensating voltages, 150r/min, no load:
(a) no compensation, (b) square method, (c) table method, (d) proposed method
$i_{ds}^s, i_{qs}^s$ [0.5A/div. , center: 0A] , $i_{ds}^r$ [0.1A/div. , center: 0A] , $V_{inv}^a$ [2.5V/div. , center: 0V], Time [100ms/div.]

the sampling noise, it seems that the harmonic distortions are not reduced in the d-axis current of the rotor reference frame in Fig. 14-d.

Hence, the d- and q- axis current in the stationary reference frame are used for the FFT analysis to examine the result. The FFT results for Fig. 14- a and d are shown in Fig. 15, and the ratio of each harmonic to the fundamental one is summarized in Table I. Although the harmonics of 11th and 13th are slightly increased, the harmonics of 5th and 7th are decreased conspicuously by the proposed method. A Selective Harmonic Distortions (SHD) can be defined as (11).

$$SHD[\%] = \frac{\sqrt{I_5^2 + I_7^2 + I_{11}^2 + I_{13}^2}}{I_1} \times 100 \qquad (11)$$

, where $I_k$ is the magnitude of $k^{th}$ order harmonic.

By (11), the SHDs of the d- and q- axis current in Fig. 15-a are 7.1% and 7.22% respectively. In the case of Fig. 15-b, those are 2.29% and 2.4%. Therefore, based on those SHDs, it can be concluded that the harmonic distortions of the output current are diminished by about 67% with the proposed method.

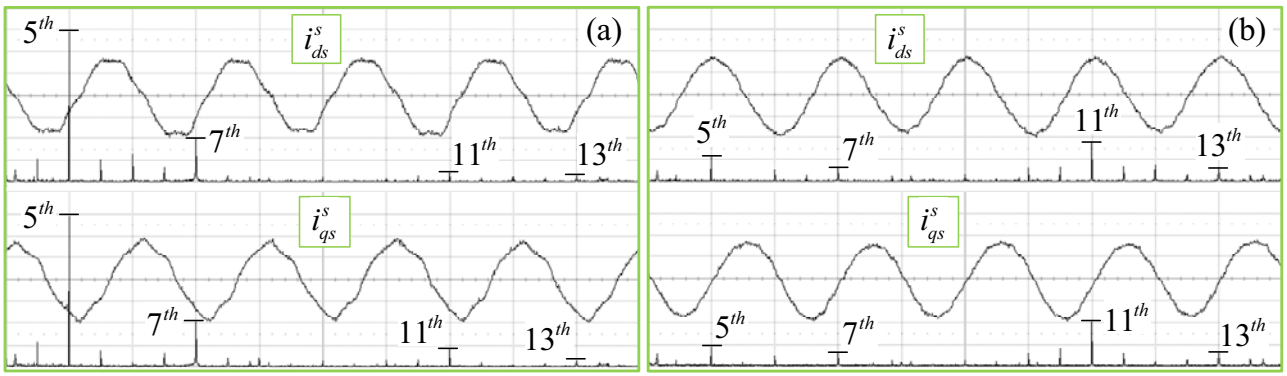


Fig. 15 FFT of output currents, 150r/min, no load: (a) no compensation, (b) proposed method
$i^s_{ds}, i^s_{qs}$ [0.6A/div. , center: 0A], Time [100ms/div.]
FFT of current [9.6mA/div. , center: 38.4mA], Frequency [5Hz/div. , center:45Hz]

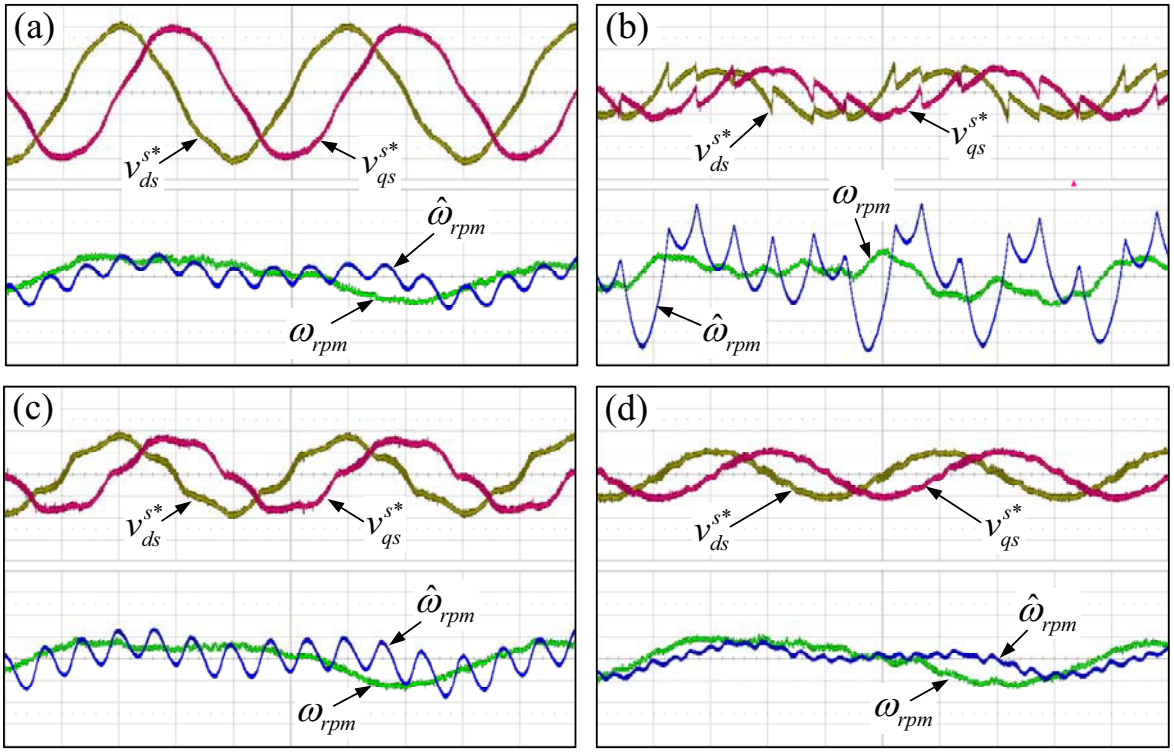


Fig. 16 Voltage references, compensating voltages, actual speed, and estimated speed, 150r/min, no load:
(a) no compensation, (b) square method, (c) table method, (d) proposed method
$v^{s*}_{ds}, v^{s*}_{qs}$ [5V/div. , center: 0V], $\omega_{rpm}, \hat{\omega}_{rpm}$ [5r/min/div. , center: 150r/min], Time [50ms/div.]

TABLE I
FFT RESULTS FOR THE OUTPUT CURRENTS IN FIG. 15

| | | Ratio to the fundamental [%] | |
|---|---|---|---|
| | | No compensation | Proposed method |
| $i^s_{ds}$ | $5^{th}$ | 6.81 | 1.128 |
| | $7^{th}$ | 1.94 | 0.628 |
| | $11^{th}$ | 0.426 | 1.798 |
| | $13^{th}$ | 0.277 | 0.575 |
| $i^s_{qs}$ | $5^{th}$ | 6.88 | 0.906 |
| | $7^{th}$ | 2.04 | 0.586 |
| | $11^{th}$ | 0.76 | 2.06 |
| | $13^{th}$ | 0.278 | 0.62 |

In Fig. 16, the voltage references and the speeds are displayed according to the compensating methods. To show distinct differences, the test motor is also driven in the same operating condition with that in Fig. 14.

As mentioned before, the voltage references are to be a balanced three-phase if the compensation is ideal. In Fig. 16-d, the voltage references in the stationary reference frame, $v^{s*}_{ds}$ and $v^{s*}_{qs}$, are closest to the sine-wave compared with the other figures in Fig. 16.

In the comparisons of each speed, it is confirmed how the non-linearity of the inverter affects the sensorless control system. The torque ripples caused by the current-harmonics can affect the actual speed, $\omega_{rpm}$. And, the distortions of the voltage references may invoke the fluctuation in each estimated speed, $\hat{\omega}_{rpm}$.

Contrary to the other figures in Fig. 16, the fluctuation of the actual speed, related to the low order harmonics, is evidently observed in Fig. 16-b. This can be considered

as the effect of the torque ripples, because the current distortions by the square method at the given condition are the worst as shown in Fig. 14-b.

In Fig. 16, based on the comparison between the estimated speed and actual speed, it is regarded that the fluctuation of the estimated speed is increased according to the voltage-distortions. Because of this fluctuation in the estimated speed, though the fluctuation is not in the actual speed, the performance of the sensorless control system can be degraded as shown in Fig. 14 and 16.

The harmonic distortions in the output currents, the voltage references, and the estimated speed are linked, and they can be mitigated by the proper compensation. As shown in Fig. 14 and 16, compared with the other compensating methods, the proposed method not only mitigates the voltage distortions but also improves the performance of the sensorless control conspicuously.

## IV. CONCLUSIONS

In this paper, a novel method has been proposed to compensate the non-linearity of the inverter. To clarify the purpose of the compensation, the non-linearity of the inverter has been modeled as the distorted voltage employing the equivalent circuit.

The trapezoidal voltage has been exploited to compensate the distorted voltage. This idea is based on the correlation between the trapezoidal angle and the harmonics of the trapezoidal voltage. By the modulation of the trapezoidal angle, the proposed method can effectively suppress the harmonic distortions, comes from the non-linearity of the inverter.

The harmonic distortions in the current-synchronous frame are observed to modulate the trapezoidal angle. Through the simple signal processing with the integral controller, the angle can be modulated. Because the saturated level of the trapezoid is measurable at stationary condition, the only tunable factor is the gain and the method is easily applicable in the field, compared with the other method employing the disturbance observer that requires electro-mechanical parameters.

To prove the validity of the proposed method, a series of experiments has been executed. The effectiveness of the proposed method has been confirmed at various operating conditions. The harmonic distortions in the output current, the voltage references, and the estimated speed have been diminished conspicuously by the proposed method.

## REFERENCES


[1] Bon-Ho Bae, Seung-Ki Sul, et al, “Implementation of Sensorless Vector Control for Super-High-Speed PMSM of Turbo-Compressor”, IEEE Trans. Ind. Appl. Vol. 39, no. 3, pp. 811-818, May/June 2003

[2] Shiegeo Morimoto, Keisuke Kawamoto, et al, “Sensorless Control Strategy for Salient-Pole PMSM Based on Extended EMF in Rotating Reference Frame”, IEEE Trans. Ind. Appl, vol. 38, no. 4, pp. 1054-1061, Jul./Aug., 2002.

[3] Jong-Woo Choi, and Seung-Ki Sul, “Inverter Output Voltage Synthesis Using Novel Dead Time Compensation”, IEEE Trans. Power Electron., vol. 11, no. 2, pp. 221-227, Mar. 1996.

[4] Gianmario Pellegrino, Radu Iustin Bojoi, et al, “Accurate Inverter Error Compensation and Related Self-Commissioning Scheme in Sensorless Induction Motor Drives”, IEEE Trans. Ind. Appl., vol. 46, no. 5, pp. 1970-1978, Sept./Oct., 2010.

[5] Jong-Woo Choi, and Seung-Ki Sul, “A New Compensation Strategy Reducing Voltage/Current Distortion in PWM VSI Systems Operating with Low Output Voltages”, IEEE Trans. Ind. Appl., vol. 31, no. 5, pp. 1001-1008, Sept./Oct., 1995.

[6] David Leggate, and Russel J. Kerkman, “Pulse-Based Dead-Time Compensator for PWM Voltage Inverters”, IEEE Trans. Ind. Electron., vol. 44, no. 2, pp. 191-197, Apr. 1997.

[7] Alfredo R. Munoz, and Thomas A. Lipo, “On-Line Dead-Time Compensation Technique for Open-Loop PWM-VSI Drives”, IEEE Trans. Power Electron., vol. 114, no. 4, pp. 683-689, Jul., 1999.

[8] N. Urasaki, T. Senjyu, et al, “Dead-time compensation strategy for permanent magnet synchronous motor drive taking zero-current clamp and parasitic capacitance effects into account”, IEE Proceedings Electric Power Appl., vol. 152, no. 4, pp. 845-853, Jul., 2005.

[9] L. M. Gong, and Z. Q. Zhu, “Modeling and Compensation of Inverter Nonlinearity Effects in Carrier Signal Injection-Based Sensorless Control Methods from Positive Sequence Carrier Current Distorion” in Conf. Rec. of IEEE ECCE, 2010, pp. 3434-3441, Sept., 2010.

[10] Sam-Young Kim, Wootaik Lee, et al, “Effective Dead-Time Compensation Using a Simple Vectorial Disturbance Estimator in PMSM Drives”, IEEE Trans. Ind. Electron., vol. 57, no. 5, pp. 1609-1614, May, 2010.

[11] Seon-Hwan Hwang, and Jang-Mok Kim, “Dead Time Compensation Method for Voltage-Fed PWM Inverter”, IEEE Trnas. Energy Convers., vol. 25, no. 1, pp. 1-10, Mar., 2010.

[12] Hyun-Soo Kim, Hyung-Tae Moon, et al, “On-Line Dead-Time Compensation Method Using Disturbance Observer”, IEEE Trans. Power Electron., vol. 18, no. 6, pp. 1336-1345, Nov. 2003.

[13] Silverio Bolognani, Luca Pretti, et al, “Repetitive-Control-Based Self-Commissioning Procedure for Inverter Nonidealities Compensation”, IEEE Trans. Ind. Appl., vol. 44, no. 5, pp. 1587-1596, Sept./Oct., 2008.

[14] Dae-Woong Chung, Joohn-Sheok Kim, et al, “Unified Voltage Modulation Technique for Real-Time Three-Phase Power Conversion”, IEEE Trans. Ind. Appl., vol. 34, no. 2, pp. 374-380, Mar./Apr., 1998.